Meso-modelling of Non-Crimp Fabric composites for coupled drape and failure analysis

G. Creech · A. K. Pickett

Abstract To date macro-analysis methods have been invariably used to analyse textile composite structures for forming and mechanical performance. Techniques such as geometric 'mapping' for the draping of textile fabrics and classical laminate analysis combined with simplified failure criteria to determine mechanical performance have formed the basis of most of these methods. The limited accuracy of the physical laws applied is appropriate to macro-analysis methods in which the fibre-matrix composite is treated as homogeneous medium. Today, however, modern high performance computers are opening new possibilities for composites analysis in which far greater detail of the composite constituent materials may be made. This paper presents Finite Elements techniques for the draping simulation of textile composites, specifically biaxial Non Crimp Fabrics, in which the complex deformation mechanisms of the dry tows and stitching may be properly modelled at the individual tow and stitch meso-level. The resulting 'deformed' Finite Element model is then used to provide a basis for accurate simulation of the impregnated composite structure. The modelling techniques for both draping and structural analysis are present, together with validation results for the study of a relatively large-scale hemisphere composite part.

G. Creech · A. K. Pickett (✉)
Cranfield University, School of Industrial and Manufacturing Science , Building 61, Cranfield, Bedfordshire MK43 OAL, UK
e-mail: a.k.pickett@cranfield.ac.uk

G. Creech
e-mail: g.l.creech.2001@cranfield.ac.uk

Introduction

In recent years new textile fabric forms have emerged for high performance cost effective composites manufacturing; amongst these biaxial Non Crimp Fabrics (NCF) having 0°/90° and ±45° fibres with tricot, or chain stitching, is a popular choice for draping complex geometrical shapes, Fig. 1. A particular advantage of NCF is the absence of crimp which enhances in-plane mechanical properties; furthermore, the through thickness stitching improves handling stability and delamination toughness. In combination with Liquid Composite Moulding technologies to infuse resin these preforms can provide cost effective, high performance composites, having highly integral and complex shapes. For accurate manufacture and design of composites parts simulation methods are needed to predict both fabric draping and final part performance of the impregnated composite.

Over the past fifty years mapping methods [1] have been partially successful to analyse drape of certain fabrics over simple geometrical shapes. These techniques are based on a simple kinematic algorithm in which the fabric is idealised as an orthogonal network of fibres with cross over points acting as fixed pin-jointed nodes. The method was originally developed for plain weave fabrics having tow interlacing that prevents relative tow sliding. In recent years enhancements have accounted for non-symmetric shear in textiles [2] and blankholder friction [3]; however, the method has limited accuracy and is essentially a geometric mapping of one shape to another that cannot properly treat many important material and processing conditions.

More recently the continuum Finite Element (FE) method has been applied to draping of various fabric types and forming operations; for example, thermoforming of UD and woven fabrics [4] and pressure draping of woven

Fig. 1 The assembly and an example of biaxial Non Crimp Fabric
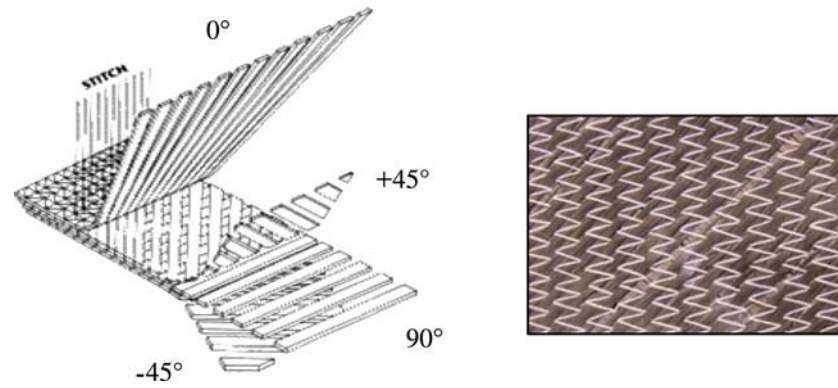
[5] and NCF [6]. The flexibility of the Finite Element method allows many variables found in composite sheet forming to be represented, such as complex tooling, friction and blankholders. The homogenised anisotropic constitutive fabric model combined with a shell element formulation can reasonably treat in-plane stretching, compression, bending, shear and shear locking. However, for analysis of individual tow slippage mechanisms, local tow compaction, stitch failure and the complex stitch-to-tow interactions a more detailed meso-mechanical modelling approach is needed.

This paper presents a meso-modelling approach for coupled drape and failure simulation of a biaxial NCF having a tricot stitch. Details of the selected NCF for this work are presented in Table 1. For draping the approach has been specifically developed to ensure that all principle deformation modes of the individual tows and stitches are represented and, importantly, that the technique is computationally efficient so that relatively large-scale structures may be analysed. For failure analysis of the impregnated composite the draped meso-mechanical FE mesh is used with material models for the impregnated tows. The tow constitutive model accounts for elastic, damage and ultimate failure. Modelling strategies for the meso-mechanical representation of NCF and procedures

for identification of material parameters for drape and failure analysis are presented, together with validation results for the full-coupled drape and impact simulation of a NCF composite hemisphere part.

Non-continuum mesoscopic fabric modelling

In order to present the modelling strategy adopted a clear understanding of the key deformation mechanisms in biaxial NCF is necessary. These mechanisms have been described [7, 8] and are shown schematically in Fig 2.

In detail the six mechanisms are:

(a) Tow compaction due to reduction in fabric area during in-plane shear, or when directly compacted by tooling constraints.

(b) In-plane fabric shear which is resisted by frictional forces at the tow contact points and stitching.

(c) Inter-tow frictional sliding which is prevalent in NCF materials due to the absence of tow inter-locking. Resistance is provided by contact to surrounding tows and the stitching.

(d) Cross-over point sliding which is also prevalent in NCF materials due to the absence of tow interlocking. Frictional resistance is provided by contact between the fibre plies.

(e) Stitch tension, since during shear deformation the stitches deform generating additional tension within the stitching and, consequently, additional friction forces.

(f) Frictional stitch sliding which occurs at stitching loop points as a result of differential tensions in adjoining sections of the stitch geometry.

(g) Stitching-to-fibre interaction.

Each of the above mechanisms is subject to coupling. For instance, in-plane shear will generate stitch tension and sliding leading to tow compaction and increased inter-tow shear friction.

Table 1 Specifications of the selected (±45°) biaxial SAERTEX NCF used to develop the meso-mechanical drape and failure models
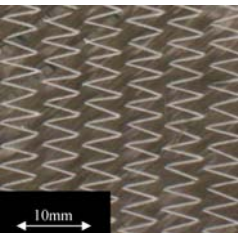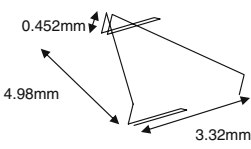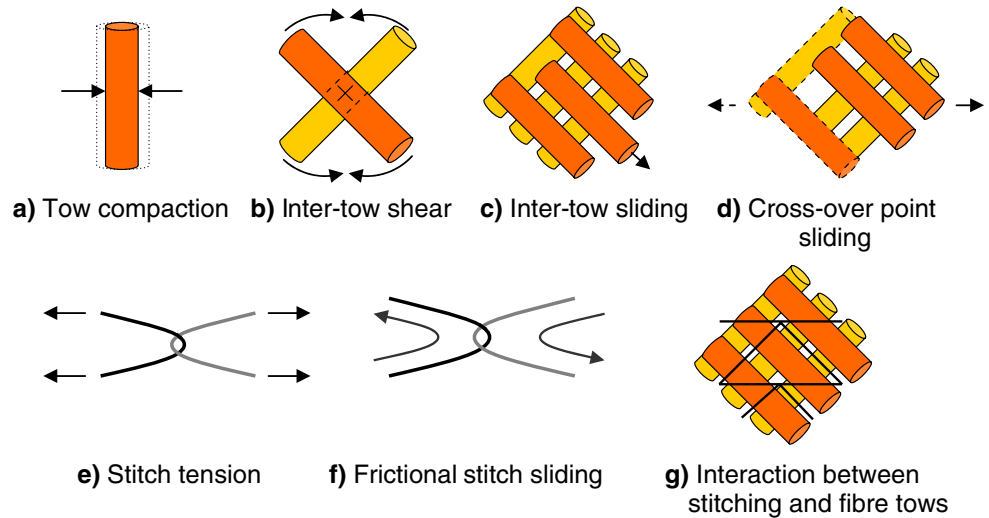
Tricot stitched biaxial (±45°) Non-Crimp Fabric	Specification
	Material: Saertex V93813 **Fabric type:** Biaxial ±45 NCF **Weight:** 321gm⁻² **Fibres:** 12K TORAY T700 carbon fibre **Stitch:** PES 76 dtex (Tricot)

Fig. 2 Mesoscopic fabric deformation mechanisms in a biaxial NCF

a) Tow compaction   **b)** Inter-tow shear   **c)** Inter-tow sliding   **d)** Cross-over point sliding

e) Stitch tension   **f)** Frictional stitch sliding   **g)** Interaction between stitching and fibre tows

Mesoscopic modelling strategy

The aim of the mesoscopic drape model is to capture all principle deformation mechanisms outlined above, but remain practical for analysis of relatively large scale structures; this has led to the following modelling approach. Each 'blanket' of biaxial NCF comprises of two separate ply layers constructed from distinct rows of solid elements to model individual tows, with interconnecting bar elements to approximate the stitching, Fig. 3. The width of each tow is similar to the real tows, but is also dictated by the location of the through-thickness stitching points. Contact and frictional sliding between the tows and stitches is treated using an appropriate contact algorithm and additional stitch-to-tow connection elements. This model has been implemented in PAM-CRASH, an explicit Finite Element simulation code.

Mesoscopic model: tow characterisation

The tow deformation behaviour must be characterised for axial, transverse and bending stiffness. Whereas the axial and bending stiffness is readily modelled, the non-linear transverse stiffness behaviour is more difficult since this is due to the complex compaction of a bundle of many individual fibres. The constitutive model used is a so-called
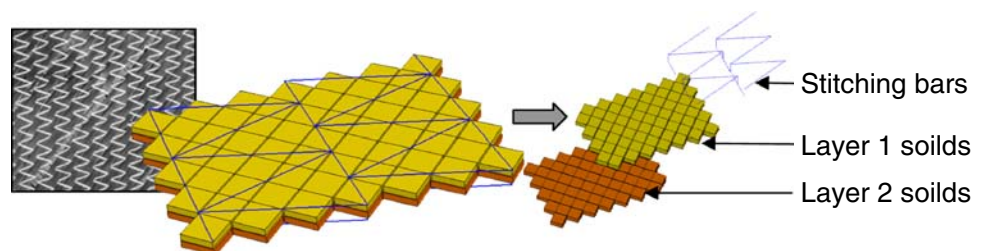
'orthotropic bi-phase' material model [9] consisting of a separate fibre $[C^{\mathrm{f}}]$ and matrix $[C^{\mathrm{m}}]$ stiffness law,

$$
[C^{\mathrm{tow}}] = [C^{\mathrm{f}}] + [C^{\mathrm{m}}] = \begin{bmatrix} E_{11}^{\mathrm{f}} & 0 & 0 \\ 0 & 0 & 0 \\ 0 & 0 & 0 \end{bmatrix}
$$
$$
+ \begin{bmatrix} E_{11}^{\mathrm{m}}/N_{\mathrm{m}} & v_{12}^{\mathrm{m}}E_{22}^{\mathrm{m}}/N_{\mathrm{m}} & 0 \\ v_{21}^{\mathrm{m}}E_{11}^{\mathrm{m}}/N_{\mathrm{m}} & E_{22}^{\mathrm{m}}/N_{\mathrm{m}} & 0 \\ 0 & 0 & G_{12} \end{bmatrix} \quad (1)
$$

where suffixes f and m denote fibre and matrix respectively; E, G and v are Young's modulus, Shear modulus and Poisson's ratio in the fibre direction 1, or transverse direction 2; N_{m} is the quantity $1 - v_{12}^{\mathrm{m}}v_{21}^{\mathrm{m}}$.

The lateral compaction of a tow is important for correct intra-fibre shear and stitch tension behaviour in the fabric during shearing. Direct measurement of lateral tow compaction is difficult and, consequently, it has been indirectly measured here using the experimental picture frame test, Fig. 4a. A numerical model of a unit cell (6.64 mm × 6.64 mm) of the picture frame test is used to calibrate the transverse tow modulii E_{22}^{m} (and E_{33}^{m}) against area normalised experimental data, Fig. 4b; in both cases with stitching removed. The numerical model uses a pin-jointed rigid frame to induce pure shear whilst maintaining free rotation

Fig. 3 A 'representative cell' of the meso-mechanical model for NCF

← Stitching bars

← Layer 1 soilds

← Layer 2 soilds

a) *The picture frame test*

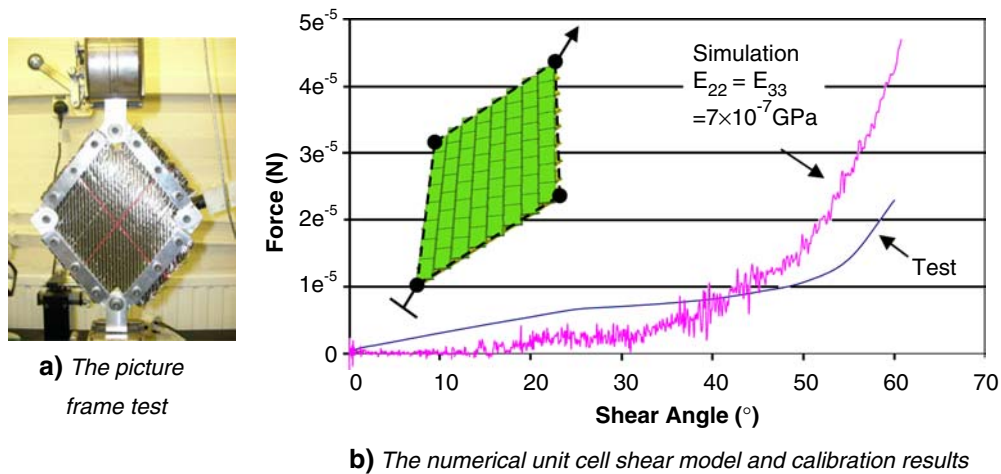**b)** *The numerical unit cell shear model and calibration results*

Fig. 4 The picture frame shear test and numerical unit-cell model for calibration of transverse tow properties

at the ends of the tows. Currently, a 'best-fit' approach is used to determine the transverse stiffness. Unfortunately the fit is not particularly good since the constant compaction modulii is not well suited to treat the non-linearly increasing stiffness of tows during compaction. The experimentally observed increased stiffness at full compaction is approximated in the numerical model via an internal contact treatment that limits final reduction in tow width.

Correct tow bending stiffness is important to correctly capture potential fabric buckling and generate correct force distributions (and frictional forces) between the fabric and tools in forming curved geometrical shapes. Calibration is performed based on the fabric flexural rigidity standard (ASTM 1388) [10] using, in this case, a single tow. From classical beam theory an initial estimate of fibre elastic modulus E_{11}^{f}, matrix elastic modulus E_{11}^{m}, and shear modulus G_{12}^{m} are computed for the measured deflection of a single tow, Fig. 5. Further calibration is necessary to fit a simulation model of the test with experimental measurements. This has provided an axial tow modulus E_{11}^{f} equal to 0.07 GPa for good bending stiffness. This is clearly much lower than the true axial modulus of 230 GPa for Toray T700 fibres; however, draping processes are conducted under low forces and using this value does not lead to unrealistic axial straining of the tows, as demonstrated later for the axial bias extension test, Fig. 13. Thus the modulus is calibrated for correct bending, rather than correct axial stiffness.
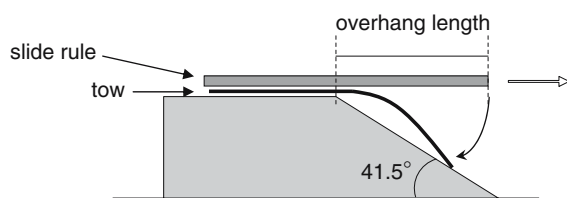

Fig. 5 Test setup for determination of tow bending stiffness

Mesoscopic model: stitch characterisation

The orientation of the tricot stitching, relative to the direction of fabric shearing, produces different shear resistance and a so-called 'shear bias' effect [6] and is due to the different loading mechanisms that the stitches undergo. This can be measured in the picture frame test by fixing the fabric in the two possible mounting directions with respect to the loading (shearing) direction, defined as 'positive' and 'negative' shear in Fig. 6a, b. The shear bias can be significant, as demonstrated by the large differences in shear resistance force for positive, negative and unstitched fabric, Fig. 6c (error bars calculated using a student *T*-test method to 90% confidence from 3 tests). Clearly, it is important that the mesoscopic model must be capable of capturing shear bias.

The bar elements used to represent the stitching have a non-linear elastic tension only law, Fig. 7a. A limitation of the current model is that stitch elements are connected at common nodes and stitch segments are uncoupled. This level of modelling cannot permit force redistribution between adjacent stitch elements or slippage of the stitches around the tows; only frictional sliding between the stitches and tows is possible. Figure 7b shows tensile coupons of NCF 250 mm long by 50 mm wide, loaded in both the 'positive' and 'negative' shear directions. The positive shear case is used to calibrate the 'I' stitches, whereas the 'negative shear' case calibrates the 'Λ' stitches in the tricot stitch style. Also given in Fig. 7 are the resistance force experimental measurements and equivalent numerical results using the techniques presented below.

Stitch bar element stiffness is based upon axial force data obtained from bias extension tests and strains determined using analytical formulae [7]. An assumption is made here that shear resistance is only dominated by the

Fig. 6 Definition of shear orientations and measurements for shear resistance for the tricot stitch NCF
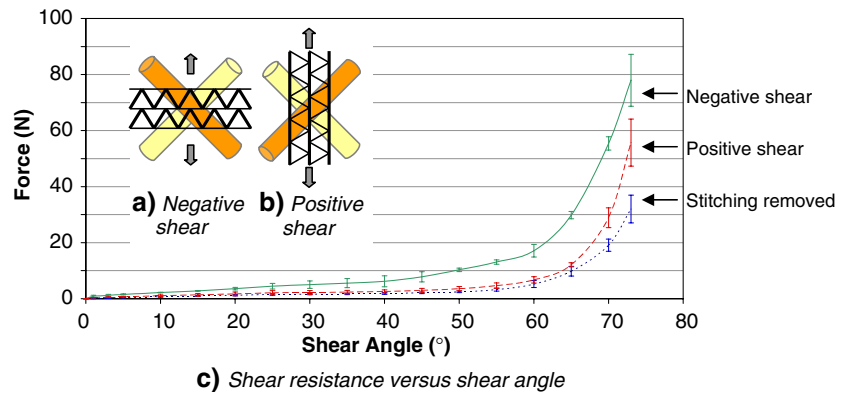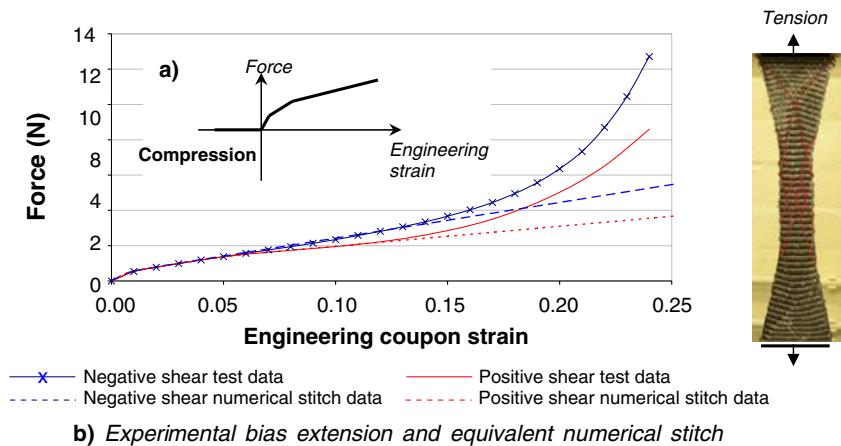

c) *Shear resistance versus shear angle*

Fig. 7 Bias extension shear test results and the stitch element material model law

**b)** *Experimental bias extension and equivalent numerical stitch*

stitches up to an inter-fibre shear angle of ~30°, above which tow compaction forces start to become significant. A non-linear stitch stiffness has therefore been calculated by comparing the bias extension axial force, normalised to the area of either 'Λ' or 'I' stitch elements in the coupon width, to stitch strain, e, data calculated using the analytical formulae, coupon and stitch definitions presented in Fig. 8. In this figure the central bias extension shear angle is θ_s caused by the coupon extension D.

$$\theta_S = \frac{\pi}{2} - 2\cos^{-1}\left(\frac{1}{\sqrt{2}} + \frac{D}{2L_{\text{eff}}}\right) \quad (2)$$

$$d(\theta_S) = \sqrt{2c_0^2 \cos^2\left(45 - \frac{\theta_S}{2}\right) + 2h_0^2 \sin^2\left(45 - \frac{\theta_S}{2}\right)} \quad (3)$$

Fig. 8 Analytical formulae, stitch and bias extension definitions for determination of stitch strains [7] during extension
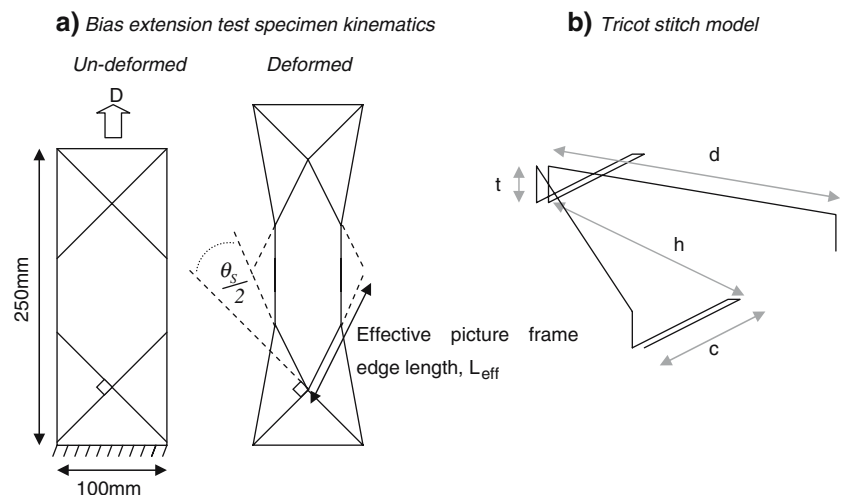
$$c(\theta_S) = \sqrt{2}c_0 \cos\left(45 - \frac{\theta_S}{2}\right) \qquad (4)$$

$$e_c = \frac{(c(\theta_S) - c_0)}{c_0} \qquad (5)$$

$$e_d = \frac{(d(\theta_S) - d_0)}{d_0} \qquad (6)$$

Mesoscopic model: tow-to-stitch interaction

The stitches wrap around tows to hold them in place. Tensile stitch forces are generated during manufacture and also during certain fabric deformations, and lead to friction interaction forces between the tows and stitches as these undergo relative sliding. This friction force is treated via connection elements joining the stitch nodes to the tow element nodes, Fig. 9a.

Mechanical data for these friction forces is determined using a 'tow pull-out test', Fig. 9b, in which a group of tows are extracted from the blanket which is held by clamps on either sides. A difference in pull-out force is measured for each fibre layer due to a varying constraint imparted by the stitching, shown in Fig. 9 (error bars calculated using a student T-test method to 90% confidence from 3 tests). Repeatability of data from this test is poor as a result of varying impalement of separate tows during the

stitching process and is shown by the large scatter in the test error bars.

Mesoscopic model: tow-to-tow and fabric-to-tool friction

Fabric forming is a contact dominated problem for which explicit Finite Element simulation methods are ideally suited. Friction between the tows and fibre plies which constitute a NCF inevitably contribute to the resistance to in-plane shear and cross-over sliding. This resistance can be treated using a frictional contact algorithm between the tows of the meso-model and defined by a simple Coulomb friction coefficient.

Static friction coefficients have been determined using the equipment shown in Fig. 10 and a Zwick Z010 tensile test machine. The contacting plates have been wrapped with unidirectional fibre tows and tested with relative fibre orientations of 0° to 90°, to characterise inter-ply contact, and 0° to 0° to characterise contact between adjacent tows within the same ply. Tests have also determined the friction coefficient between the NCF fabric and aluminium tooling used during draping trials (described later).

$$\frac{F}{P} = \mu \qquad (7)$$

Table 2 summarises the contact pressures resulting from the force, P, and crosshead velocities tested. Mean average friction coefficients, μ, from tests using these variables have been calculated using Eq. 7 and are shown in Table 3. The low standard deviations indicate kinetic

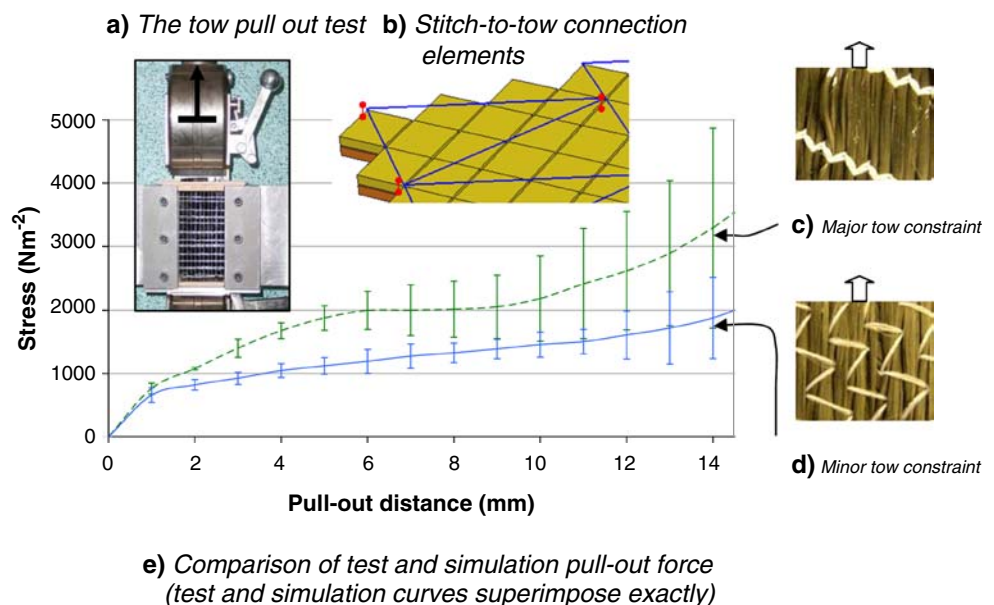**Fig. 9** Tow pull-out test and numerical results

a) *The tow pull out test* b) *Stitch-to-tow connection elements*

c) *Major tow constraint*

d) *Minor tow constraint*

e) *Comparison of test and simulation pull-out force (test and simulation curves superimpose exactly)*

Fig. 10 Friction testing
equipment and formulae
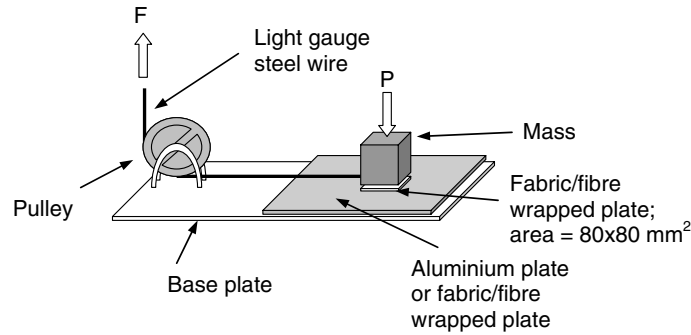
Table 2 Friction test variables

Pressure (N/m^2)	1370	3700	6500
Crosshead velocity (mm/min)	25	300	1000

Table 3 Friction test results

Contact interfaces	μ	Standard deviation
Tow–tow 0°–90°	0.18	0.006
Tow–tow 0°–0°	0.035	0.019
Fabric – aluminium	0.25	

fibre friction is not dependent on contact pressure or velocity.

Bias extension simulation results and test comparisons

The bias extension test provides a simple, yet challenging test to evaluate the proposed mesoscopic fabric model because of the wide range of deformation mechanisms that occur. This validation study uses 250 mm long by 100 mm wide coupons of biaxial NCF, Table 1, loaded axially with fibres laid in the ±45° directions. Both positive and negative shear is investigated. Figure 11 shows the deformed fabric (negative shear case) and illustrates the different deformation zones that occur and must be captured by the meso-mechanical model.
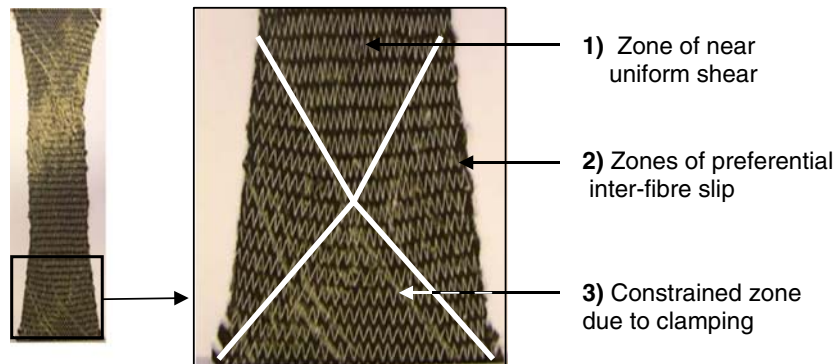
The Finite Element mesh, together with loading and boundary conditions used to replicate the test coupon are shown in Fig. 12. A total of 36000 solid and 21000 bar elements are used to model the tows and stitching.

Figure 13 shows a good agreement between deformation mechanisms observed for the test and the mesoscopic fabric model. The numerical model correctly predicts the three distinct deformation zones identified previously in Fig. 11 and of specific interest is correct simulation of preferential inter-tow slippage (zone 2) that occurs between the constrained (zone 3) and the region of near pure shear (zone 1). A reduction of inter-fibre angle towards the free specimen edges within the central shear zone is also reproduced and demonstrates the complexity of the fabric deformation mechanisms that occur within the specimen.

Figure 14 compares test, simulation and analytical predictions for positive and negative inter-fibre shear angle at the centre of the specimen. In each case the simulation shows improved agreement to test in comparison to the analytical model. The theoretical model tends to show an incorrect locking phenomenon in the latter stages of deformation since inter-tow slip mechanisms, which occur in practice, are not treated. Furthermore, the analytical formula

Fig. 11 Bias extension fabric
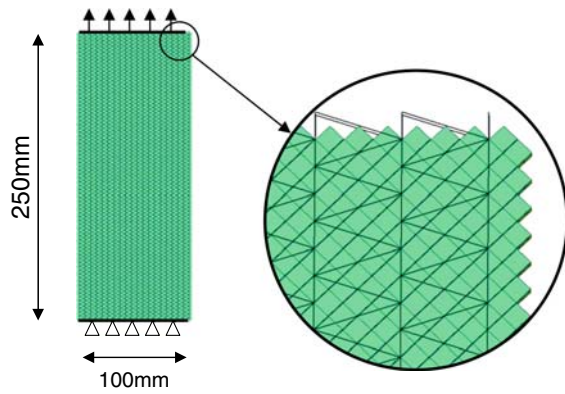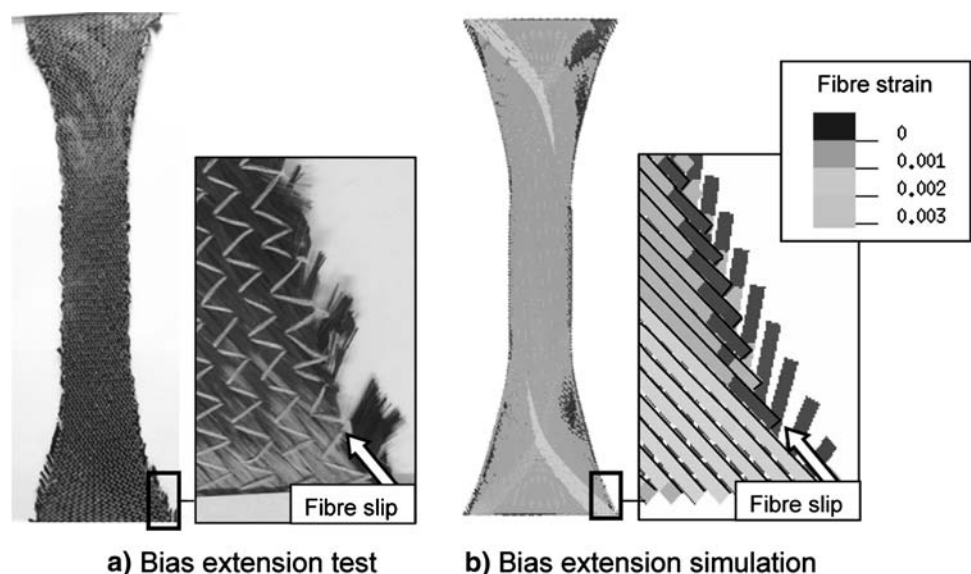test and deformation zones

1) Zone of near uniform shear

2) Zones of preferential inter-fibre slip

3) Constrained zone due to clamping

Fig. 12 The bias extension simulation model: Mesh, dimensions, boundary conditions and loading for the positive shear case

incorrectly gives identical results for both cases since the method is based on geometrical consideration and not material behaviour. The results are over predicted due to neglect of inter-tow (or stitch) sliding which occurs in practice. This model is reasonably valid for woven fabrics but only approximate for stitched NCF's at low shear angles.

The simulation results of resistance force for the coupon under positive and negative shear provide encouraging comparison with test measurements, Fig. 15. In each case the lower simulation force levels are attributed to the approximation of pure shear in the stitch strain model which is not truly representative of stitch deformation observed during tests, Fig. 16.

In addition, the uncoupled strain between stitch segments cannot fully compact the tows, or locally redistribute loading in the stitch bar elements as occurs in practice. This effect is most significant in positive shear, at higher coupon strains, due to the limited compaction of tows.

Draping simulation of a hemisphere

The following study involves draping the biaxial NCF over a hemispherical metal punch with a blankholder to maintain fabric tension and prevent wrinkling. The study provides a further validation of the proposed meso-mechanical draping model applied to a process that is representative of real fabric forming. In addition this study is also used to demonstrate how the deformed fabric FE mesh may be used as a basis to perform accurate meso-mechanical failure analysis of impregnated composites.

The hemisphere study: drape testing

The test setup is shown in Fig. 17, together with intermediate forming stages and a final view of the deformed fabric. The diameter of the metal punch is 156 mm, the applied blankholder pressure is 3.35 kPa and the rate of loading is 10 mm/min in an Instron Z010 compression testing machine.

Test and simulation results for the hemisphere study

A meso-mechanical Finite Element simulation of the hemisphere forming was performed using 120,000 solid and 70,000 bar elements for the tows and stitching. The simulation first involved loading the fabric with the blankholder to the required pressure prior to forming with the metal hemisphere at a loading rate of 1 m/s. This is significantly faster than the quasi-static experiment; this is necessary to reduce computational time and is a standard practice in metal and composites forming simulation using an explicit Finite Element code. Figure 18 shows the deformed FE mesh after final forming and also gives

Fig. 13 Comparisons of global and local deformations for the test and simulation bias extension coupons (positive shear case loaded to 28% engineering strain)

a) Bias extension test   b) Bias extension simulation

Fig. 14 Comparison of bias extension central inter-fibre angle for (**a**) positive and (**b**) negative shear; test, simulation and analytical predictions
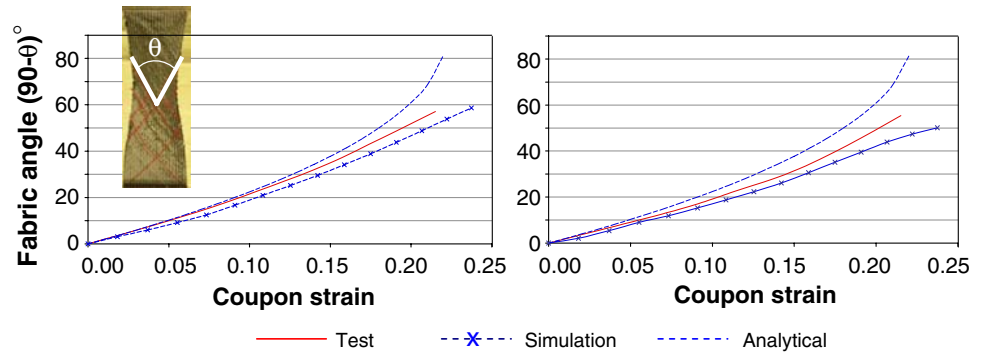

Fig. 15 Comparison of test and simulation bias extension resistance force for (**a**) positive shear and (**b**) negative shear
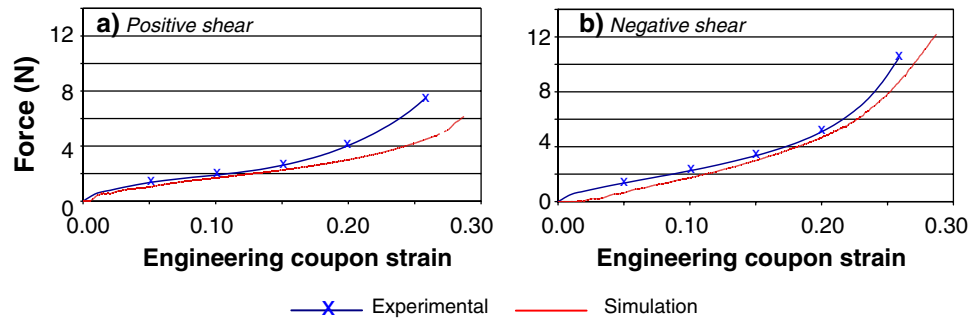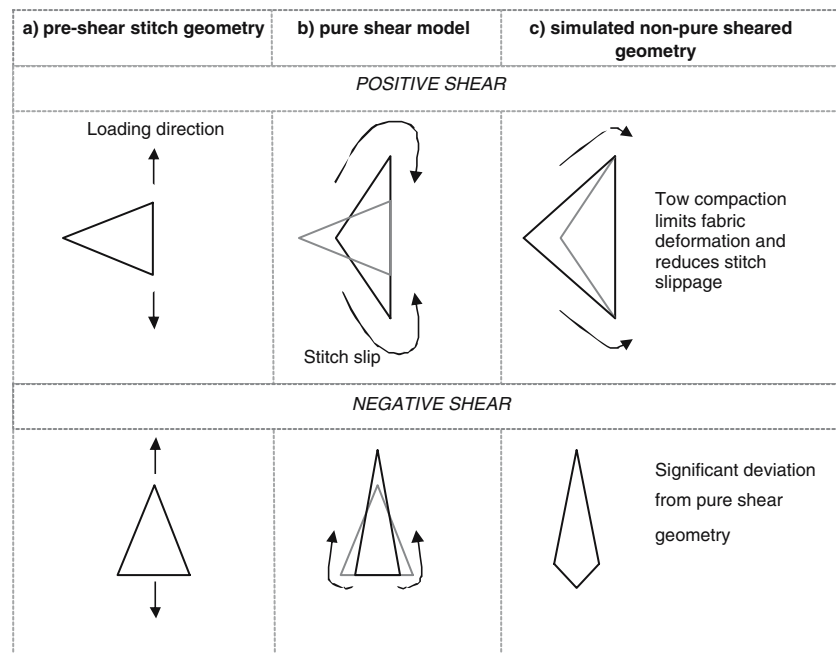

Fig. 16 Deviation of stitch geometry from pure shear during bias extension tests

results for variation in fabric shear angle around the hemisphere at 40 mm height (measured from the plane of the blankholder) for test, macro- and meso-FE simulation.

The test and meso-simulation show an excellent agreement and, importantly, the numerical model correctly predicts differences in maximum shear angle in each quadrant of the hemisphere, which is due to fabric shear bias identified for this NCF, described previously in section 2.3. The macro- FE model (not shown) used the PAM-FORM software [11, 12] with shell elements and a homogenised anisotropic constitutive fabric law and cannot detect this trend.

Coupling, mechanical data and meso-mechanical failure analysis for the hemisphere

In order to evaluate meso-mechanical failure analysis the draped hemisphere part was investigated further. The

Fig. 17 Test setup and forming of the biaxial NCF using a hemispherical metal punch and blankholder restraint
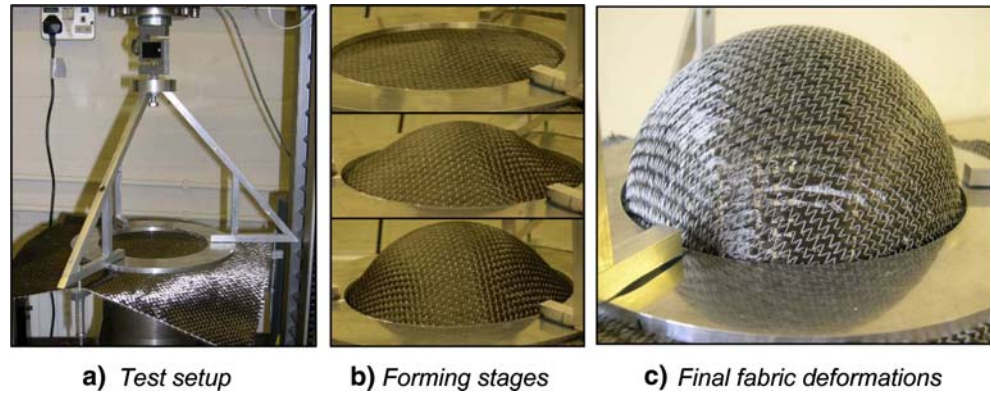

a) *Test setup*　　**b)** *Forming stages*　　**c)** *Final fabric deformations*

Fig. 18 Final deformed mesh for the meso-mechanical model and comparison of fabric shearing for test, macro- and meso-mechanical FE analysis

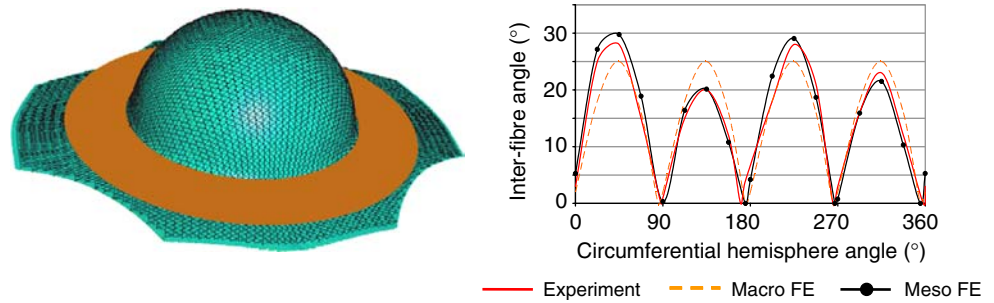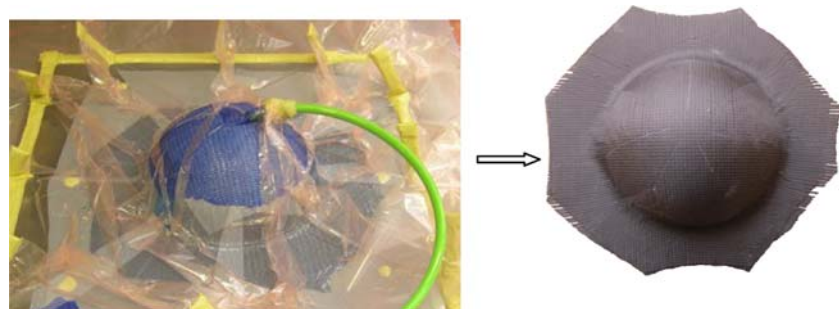Experiment　– – – Macro FE　Meso FE

Fig. 19 Manufacture of the impregnated hemisphere part using the VARI process

draped hemisphere fabric was impregnated with resin (Araldite LY3505/XB3404) using Vacuum Assisted Resin Infusion (VARI) to obtain the final part shown in Fig. 19.

The draped hemisphere simulation results are easily converted into a solid composite model having the same orthotropic material model previously described by Eq. 1. For simulation of the component mechanical performance the dry tow data is substituted for elastic and failure properties of impregnated tows.

Tensile data for both resin and fibres have been obtained from datasheets available for the resin and fibre components defined. Compressive failure data has been assumed to be ~60% of the tensile data as recorded from tests of unidirectional materials [13]. Failure simulations of a single element test case loaded under transverse and longitudinal loading in tension and compression compare very well to the required data, Fig. 20.

The crushing of the hemisphere is performed using a rigid punch of 50 mm diameter at a speed of 1.5 m/s, as shown in Fig. 21. In general an encouraging agreement is obtained between test and simulation for the overall deformations and the crush force versus displacement. A closer inspection of the deformations and failure modes, however, does show some differences with the test having greater compression failure of the tows and the simulation having more intra-ply shear failure. It is believed this is due to limitations in the current tow failure model and further work is studying this aspect.

Fig. 20 Failure curves in tension and compression for transverse and longitudinal loads
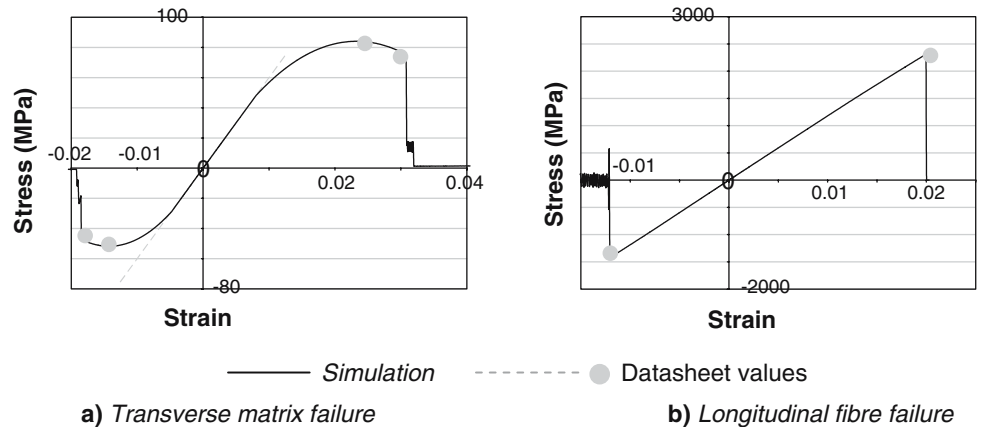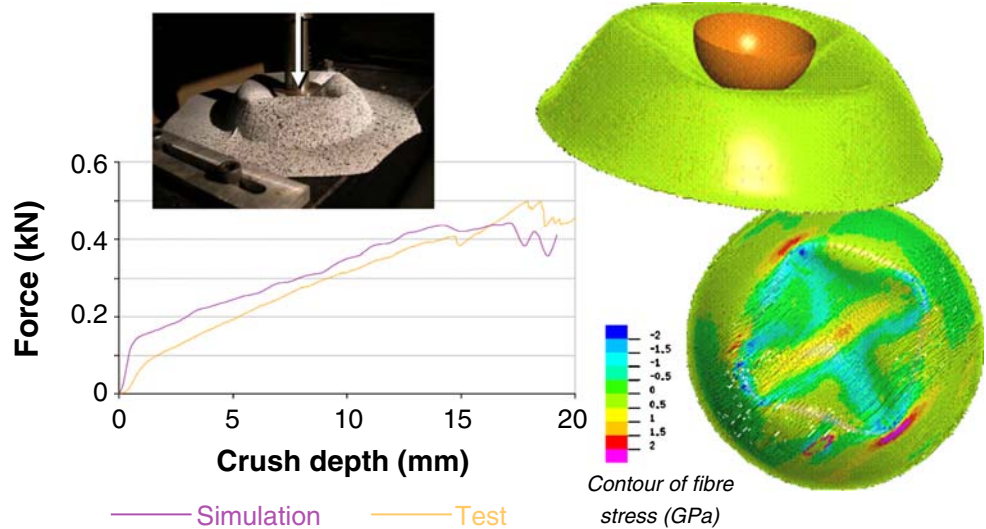

a) *Transverse matrix failure*   b) *Longitudinal fibre failure*

Fig. 21 Comparison of test and simulation for failure loading of the impregnated hemisphere part

Contour of fibre stress (GPa)

Conclusions

A new meso-mechanical Finite Element model for drape simulation of textile fabrics (NCF) has been presented that includes all the important fabric deformation mechanisms. Some limitations in the current model have been noted; in particular, an improved constitutive model for tows that decouples axial, bending and non-linear transverse compaction stiffness and techniques to allow redistribution of local stitch forces due to slip mechanisms that occur would improve accuracy. Never-the-less the model has proven successful for complex draping and provides far greater information on fabric deformations than previously possible using mapping techniques or homogenised material laws and continuum shell (or membrane) Finite Elements. Particularly encouraging has been the ability of the meso-model to capture shear bias for the hemisphere analysis.

The drapeing model also provides a unique basis to perform failure analysis of impregnated composite parts with accurate deformed fabric architectures. Coupling of process and mechanical performance is readily achieved by using the deformed fabric FE mesh for the structural analysis with alternative stiffness-failure material laws to represent the impregnated composite materials. This methodology has been successfully demonstrated for the failure analysis of the hemisphere part.

References

1. Mack C, Taylor HM (1956) J Textile Inst 47(8):477
2. Long AC (2001) The 4th International ESAFORM Conference on Material Forming. Liege, Belgium, p 99
3. Long AC, Wiggers J, Harrison P (2005) The 8th International ESAFORM Conference on Material Forming. Vol. 2, Cluj-Napoca, Romania, p 939
4. Pickett AK, Cunningham JE, de Luca P, Johnson AF, Lefebure P, Mallon P, Sunderland P, Ó Brádaigh CM, Vodermeyer A, Werner W (1996) Numerical Techniques for the Pre-Heating and Forming Simulation of Continuous Fibre Reinforced Thermo-plastics. SAMPE, Basel, Switzerland
5. Boisse P, Gasser A, Hivet G (2001) Composites: Part A 32:1395

6. Creech G, Pickett AK, Greve L (2003) The 6th International ESAFORM Conference on Material Forming. Salerno, Italy, p 863

7. Wiggers J, Long A, Harrison P, Rudd C (2003) The 6th International ESAFORM Conference on Material Forming. Salerno, Italy, p 851

8. Harrison P, Clifford MJ, Long AC (2004) Composites Sci Technol 64:1453

9. PAM-CRASH Theory Manual 2000, *ESI Group*, 99 Rue des Solets, Silic 112, 94513 Rungis-Cedex, France

10. ASTM D1388–96[E1]. Standard test for Stiffness of Fabrics

11. PAM-FORM, *ESI Group*, 99 Rue des Solets, Silic 112, 94513 Rungis-Cedex, France

12. Pickett AK, Creech G, de Luca P (2005) Revue Européenne des Éléments finis (REEF). 14(6–7):677

13. Kaw K (1997) Mechanics of composite materials. CRC Press LLC, Florida